Part V.

Appendix

A. Basis Sets used in FHI-aims

	Si	Cu	Co	Ar
minimal	[Ne]+$3s^2 3p^2$	[Ar]+$3d^{10}4s^1$	[Ar]+$3d^7 4s^1$	[Ar]
tier1	H($3d$, 4.2)	Cu^{2+}($4p$)	H($3p$, 5.8)	Ar^{2+}($3d$)
	H($2p$, 1.4)	H($4f$, 7.2)	H($4f$, 8.2)	Ar^{2+}($4p$)
	H($4f$, 6.2)	H($3s$, 2.6)	H($3d$, 5.4)	H($4f$, 7.4)
	Si^{2+}($3s$)*	H($3d$, 4.9)	H($5g$, 12.0)	H($3s$, 4.5)
		H($5g$, 10.4)	Co^{2+}($4s$)*	
tier2	H($3d$, 9.0)*	H($4p$, 5.8)	Co^{2+}($4p$)*	H($4d$, 7.8)
	H($5g$, 9.6)	H($6h$, 14.8)	H($6h$, 16.4)	H($5g$, 10.4)
	H($4p$, 4.0)	H($5s$, 10.4)	H($4d$, 5.6)	Ar^{2+}($3p$)
	H($1s$, 0.65)	H($3d$, 2.9)	H($4f$, 17.2)	H($1s$, 15.2)*
	H($4f$, 8.2)	H($4f$, 15.2)	H($1s$, 0.75)	
tier3	Si^{2+}($3d$)	H($3d$, 3.6)	H($4d$, 7.8)	H($4d$, 5.8)*
	H($3s$, 2.6)	H($3s$, 25)	H($2p$, 5.8)	H($5f$, 9.2)
	H($3d$, 3.4)	H($3p$, 2.3)	H($4f$, 8.0)	H($4s$, 11.2)
	H($3p$, 3.0)	H($5f$, 8.4)	H($5g$, 11.6)	H($5p$, 10.8)
	H($4p$, 6.4)	H($6g$, 12.4)	H($4s$, 4.3)	
	H($5g$, 10.8)			
	...	...	...	...

Table A.1.: Radial basis functions used in FHI-aims as they were selected during the basis optimization for the elements studied in this work Si, Cu, Co and Ar. "H(nl,z)" denotes a hydrogen-like basis function for the bare Coulomb potential z/r, including its radial and angular momentum quantum numbers n and l. X^{2+}(nl) denotes a n,l radial function of a doubly positive free ion of species X. The radial functions marked with an asterisk have artificially been swapped to retain the otherwise consistent order into successive angular momentum shells ("tiers", see section 5). The minimal basis set simply contains the atomic functions according to the ground-state electronic configuration of the corresponding species.

The radial basis functions (each with ($2l$+1) angular momentum functions) employed

in the present work together with their explanation are summarized in Table A.1. Apart from two exceptions, where in each case two basis functions have been artificially swapped, all angular momenta appeared naturally during the basis set generation procedure in the first tier. In the third tier, where improvements in the total energy lie only in the meV range, the order of the angular momenta is more or less arbitrary. The additional "minimal+*spd*" basis set, employed in chapter 9, is simply the tier1 set without the expensive f and g radial functions, which correspond to 7 and 9 basis functions, respectively. The bond distances $\{d_i\}$ used in the basis set generation according to Eq. 5.25 are spread to sample the self-consistent PW-LDA binding curve of the non-polarized dimer and are illustrated in Fig. A.1. We note that PW-LDA is unphysical for the Ar dimer since the latter is bound by pure van-der-Waals forces. In the basis set construction, however, it can still be used to simulate some kind of bonding to which the basis set is then optimized. Of course, in practical applications, extra care has to be taken whether a used tier is really converged.

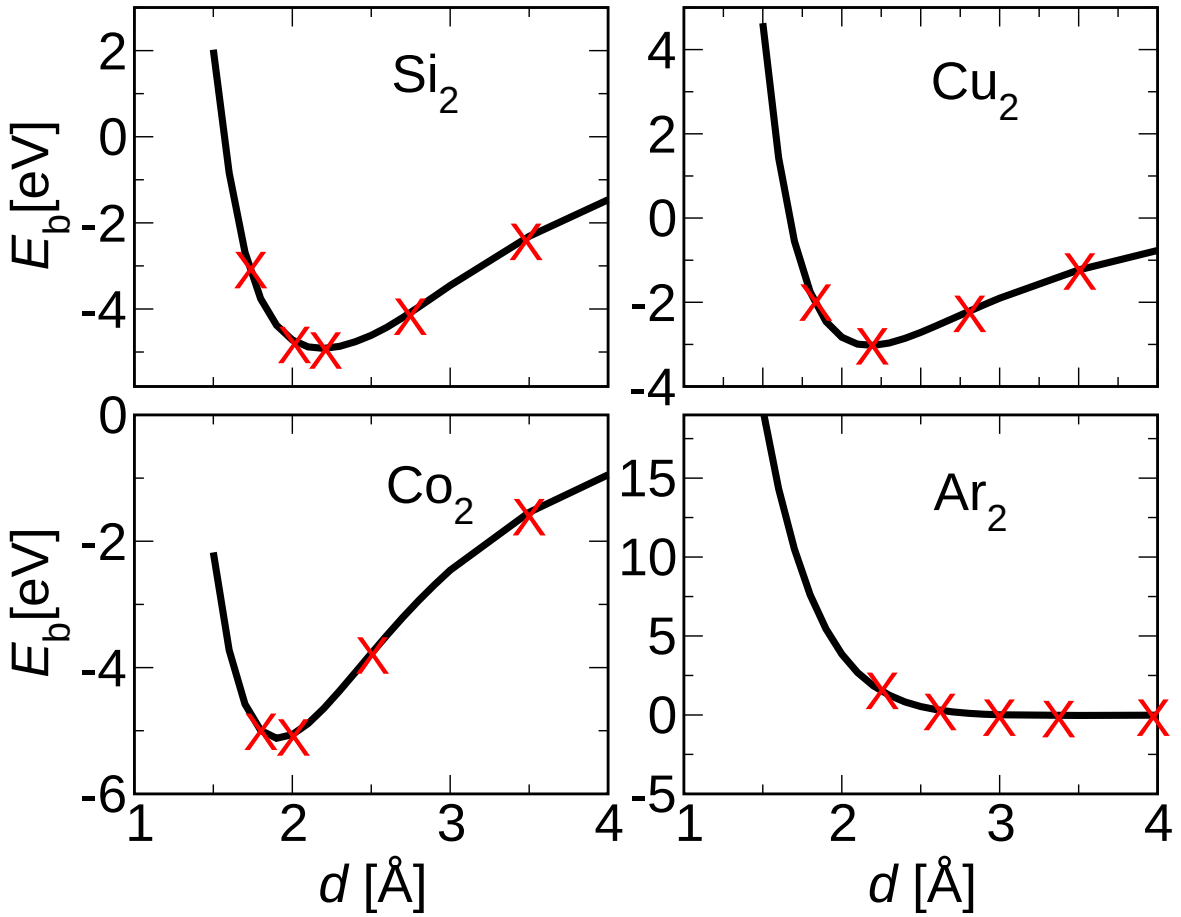

Figure A.1.: PW-LDA binding curves for basis set generation using a converged tier3 basis set to illustrate the chosen bond distances (marked by red crosses). d_i[Å]= $\{1.75, 2.0, 2.25, 2.75, 3.5\}$ for Si, d_i[Å]= $\{1.8, 2.2, 2.8, 3.5\}$ for Cu, d_i[Å]= $\{1.8, 2.0, 2.5, 3.5\}$ for Co, d_i[Å]= $\{2.25, 2.625, 3.0, 3.375, 4.0\}$ for Ar. All technical parameters are converged ($N_{\mathrm{ang,max}}$=302, $N_{\mathrm{r,div}}$=2, l_{max}=6, r_{cut}=5 Å, cf. Appendix B and C).

B. Convergence Tests for the Co_n^+Ar Complexes

The technical parameters to converge together with their default values in brackets are:

1. The integration grid which is determined by $N_{\mathrm{r,div}}$ (2) and $N_{\mathrm{ang,max}}$ (302). Cf. section 5.3.
2. The basis set (tier2). Cf. section 5.2.
3. The cutoff radius r_{cut} (5 Å). Cf. section 5.2.
4. The maximum angular momentum in the multipole decomposition of the Hartree potential l_{max} (6). Cf. section 5.4.
5. The force convergence criterium F_{max} (10^{-2} eV/Å). Cf. section 6.2.
6. The step width Δ (10^{-3} Å) for the finite displacement to calculate the Hessian and dipole derivatives. Cf. section 6.3.

For the ensuing convergence tests, each parameter is in turn individually varied whereas for the other parameters the default value is used and kept fixed. As will be shown below, these default settings are converged and have therefore been used in the production runs. All tests are done using the PBE functional. For the convergence tests, it is crucial to choose proper target quantities with respect to which the settings have to be converged, which in turn depends upon the actual problem to tackle. The starting point for the study of IR spectra of Co_n^+Ar complexes are isomers that are obtained from first-principles basin-hopping, both the bare Co clusters as well as the Co_n^+Ar complexes. Consequently, the corresponding energy differences ΔE between different isomers of the bare clusters and the complexes with Ar, respectively, need to be converged as well as the bond distances. Since we are interested in IR spectra, the frequencies ω together with the IR activities are additional target quantities. We therefore explicitly checked the convergence of the frequencies and the overall IR spectrum. Furthermore, the Ar binding energy was in the focus of interest, which is thus explicitly checked as well. The convergence tests focus on the the ground-state isomers of Co_4^+Ar and Co_6^+Ar, as well as a higher-lying isomer of each (see Fig. B.1). The bond distances, Ar binding energies, vibrational frequencies and IR spectra are considered for the ground-state isomers of the Co_n^+Ar complexes, whereas the energy differences are considered between the ground states and higher-lying isomers of the bare Co_n^+ clusters and additionally the Co_n^+Ar complexes. For the first four parameters, that are species-dependent, first the Co setting

has been converged with the Ar setting kept fixed. In a second step, the corresponding Ar setting has been varied with a fixed Co setting.

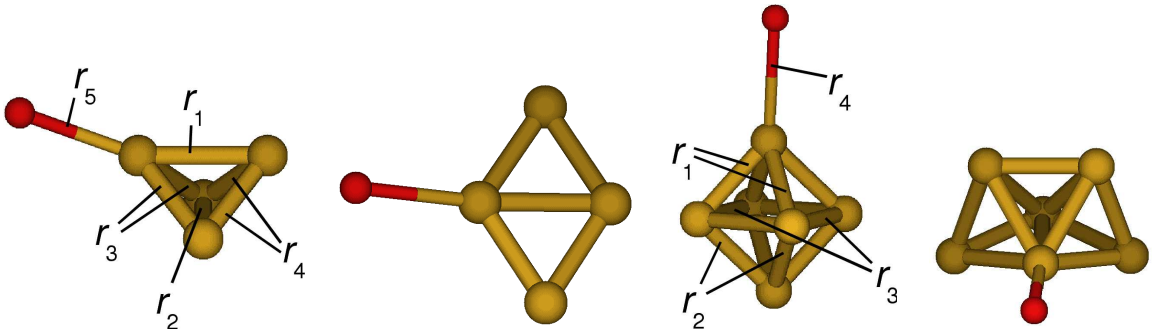

Figure B.1.: Co_n^+Ar-complexes used for the convergence tests. From left to right: ground-state isomer D_{2d} of Co_4^+Ar (S=7/2), higher-lying D_{2h} isomer (S=9/2), ground-state isomer D_{3d} of Co_6^+Ar (S=15/2), higher-lying C_{2v} isomer (S=13/2). Some bonds of the ground-state isomers are labelled that are used for the convergence tests.

B.1. Integration Grid

The angular part of the integration grid $N_{\mathrm{ang,max}}$ is varied over several different Lebedev-grids, that are 194, 302, 434, 590 and 770. Using 302 the radial part which is determined by $N_{\mathrm{r,div}}$ is augmented from 2 to 4. The convergence tests are summarized in Tables B.1, B.2, B.3, B.4 as well as in Fig. B.2.

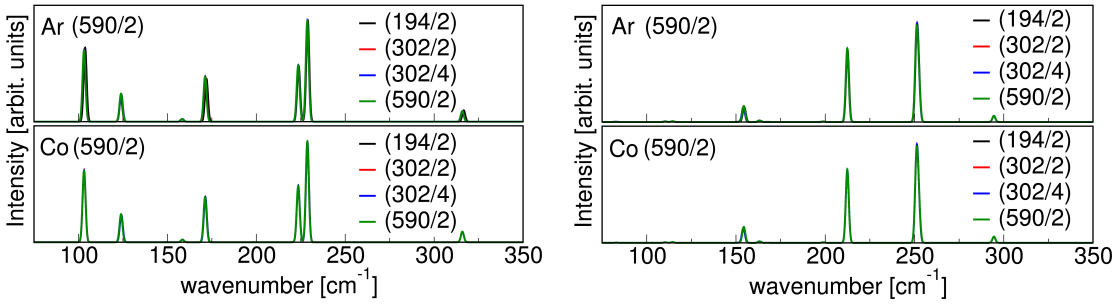

Figure B.2.: IR spectrum of the ground state of Co_4^+Ar (left panels) and Co_6^+Ar (right panels) vs. integration grid ($N_{\mathrm{ang,max}}/N_{\mathrm{r,div}}$). In the upper panels, the Ar integration grid is kept fixed, while the Co grid is varied. In the lower panels, vice versa.

As one can see, the integration grid is completely uncritical and convergence seems to be reached already for the smallest setting (194/2). For the production runs, we chose (302/2). We note that due to the adaptive grid scheme, this does not mean that the overall computational time is enhanced by a factor of 1.5, since $N_{\mathrm{ang,max}}$ actually denotes only the maximum amount of angular integration points per radial shell that is possible.

Co-/Ar-grid	$\Delta E_{\mathrm{CoN+Ar}}$	$\Delta E_{\mathrm{CoN+}}$	E_{b}	ω_{lowest}	$\omega_{\mathrm{main,1}}$	$\omega_{\mathrm{main,2}}$	$\omega_{\mathrm{largest}}$
(194/2) / (590/2)	0.562	0.537	0.303	27	224	229	317
(302/2) / (590/2)	0.562	0.536	0.303	30	224	229	316
(434/2) / (590/2)	0.562	0.536	0.303	30	224	229	316
(590/2) / (590/2)	0.562	0.537	0.303	29	224	229	316
(770/2) / (590/2)	0.562	0.537	0.303	30	224	229	316
(302/4) / (590/2)	0.562	0.536	0.303	30	224	229	316
(590/2) / (194/2)	0.562	-	0.303	30	224	229	316
(590/2) / (302/2)	0.562	-	0.303	30	224	229	316
(590/2) / (434/2)	0.562	-	0.303	30	224	229	316
(590/2) / (590/2)	0.562	-	0.303	29	224	229	316
(590/2) / (770/2)	0.562	-	0.303	30	224	229	316
(590/2) / (302/4)	0.562	-	0.302	30	224	229	316

Table B.1.: Convergence of the energy difference $\Delta E_{\mathrm{CoN+Ar}}$ [eV] between the D_{2d}- and D_{2h} isomers of Co_4^+Ar as well as between the corresponding bare clusters $\Delta E_{\mathrm{CoN+}}$ [eV], the Ar binding energy of the ground-state isomer D_{2d} of Co_4^+Ar and the lowest, largest and two main vibrational frequencies ω [cm^{-1}] of the D_{2d} isomer of Co_4^+Ar with respect to the integration grid ($N_{\mathrm{ang,max}}/N_{\mathrm{r,div}}$).

Co-/Ar-grid	$\Delta E_{\mathrm{CoN+Ar}}$	$\Delta E_{\mathrm{CoN+}}$	E_{b}	ω_{lowest}	$\omega_{\mathrm{main,1}}$	$\omega_{\mathrm{main,2}}$	$\omega_{\mathrm{largest}}$
(194/2) / (590/2)	0.445	0.561	0.116	17	213	251	295
(302/2) / (590/2)	0.442	0.559	0.116	15	212	251	295
(434/2) / (590/2)	0.441	0.558	0.115	17	213	251	295
(590/2) / (590/2)	0.442	0.559	0.117	17	212	251	295
(770/2) / (590/2)	0.441	0.559	0.115	18	213	251	295
(302/4) / (590/2)	0.442	0.559	0.116	15	212	251	295
(590/2) / (194/2)	0.442	-	0.116	19	212	251	295
(590/2) / (302/2)	0.442	-	0.116	19	212	251	295
(590/2) / (434/2)	0.442	-	0.116	17	212	251	295
(590/2) / (590/2)	0.442	-	0.117	17	212	251	295
(590/2) / (770/2)	0.442	-	0.116	19	212	251	295
(590/2) / (302/4)	0.442	-	0.116	19	212	251	295

Table B.2.: Convergence of the energy difference $\Delta E_{\mathrm{CoN+Ar}}$ [eV] between D_{3d}- and C_{2v} isomers of Co_6^+Ar as well as between the corresponding bare clusters $\Delta E_{\mathrm{CoN+}}$ [eV], the Ar binding energy of the ground-state isomer D_{3d} of Co_6^+Ar and the lowest, largest and two main vibrational frequencies ω [cm^{-1}] of the D_{3d} isomer of Co_6^+Ar with respect to the integration grid ($N_{\mathrm{ang,max}}/N_{\mathrm{r,div}}$).

Co-/Ar-grid	r_1	r_2	r_3	r_4	r_5
(194/2) / (590/2)	2.51	2.49	2.18	2.16	2.45
(302/2) / (590/2)	2.51	2.49	2.18	2.16	2.45
(434/2) / (590/2)	2.51	2.49	2.18	2.16	2.45
(590/2) / (590/2)	2.51	2.49	2.18	2.16	2.45
(770/2) / (590/2)	2.51	2.49	2.18	2.16	2.45
(302/4) / (590/2)	2.51	2.49	2.18	2.16	2.45
(590/2) / (194/2)	2.51	2.49	2.18	2.16	2.45
(590/2) / (302/2)	2.51	2.49	2.18	2.16	2.45
(590/2) / (434/2)	2.51	2.49	2.18	2.16	2.45
(590/2) / (590/2)	2.51	2.49	2.18	2.16	2.45
(590/2) / (770/2)	2.51	2.49	2.18	2.16	2.45
(590/2) / (302/4)	2.51	2.49	2.18	2.16	2.45

Table B.3.: Convergence of the bond distances [Å] with respect to the integration grid ($N_{\mathrm{ang,max}}/N_{\mathrm{r,div}}$) for the ground-state isomer D_{2d} of Co_4^+Ar.

Co-/Ar-grid	r_1	r_2	r_3	r_4
(194/2) / (590/2)	2.37	2.27	2.26	2.76
(302/2) / (590/2)	2.37	2.27	2.26	2.76
(434/2) / (590/2)	2.37	2.27	2.26	2.76
(590/2) / (590/2)	2.37	2.27	2.26	2.74
(770/2) / (590/2)	2.37	2.27	2.26	2.76
(302/4) / (590/2)	2.37	2.27	2.26	2.76
(590/2) / (194/2)	2.37	2.27	2.26	2.76
(590/2) / (302/2)	2.37	2.27	2.26	2.76
(590/2) / (434/2)	2.37	2.27	2.26	2.76
(590/2) / (590/2)	2.37	2.27	2.26	2.74
(590/2) / (770/2)	2.37	2.27	2.26	2.76
(590/2) / (302/4)	2.37	2.27	2.26	2.76

Table B.4.: Convergence of the bond distances [Å] with respect to the integration grid ($N_{\mathrm{ang,max}}/N_{\mathrm{r,div}}$) for the ground-state isomer D_{3d} of Co_6^+Ar.

B.2. Basis Set Convergence

The basis set composition is given in Appendix A. The convergence tests are summarized in Tables B.5, B.6, B.7, B.8 and Fig. B.3.

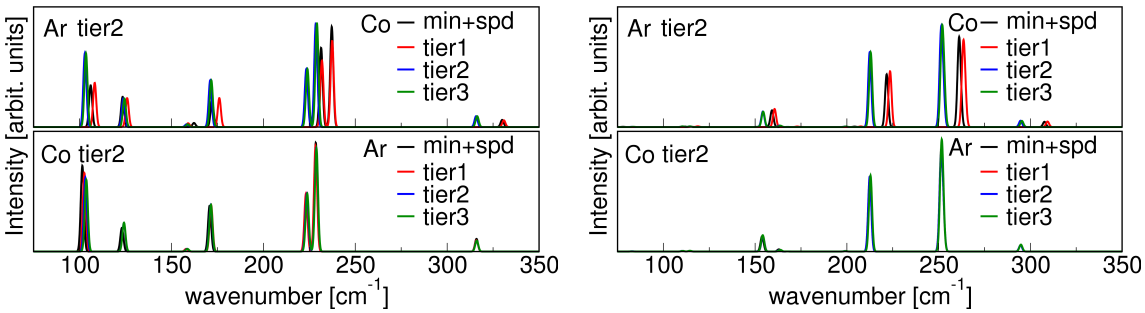

Figure B.3.: IR spectrum of the ground state of Co_4^+Ar (left panels) and Co_6^+Ar (right panels) vs. the basis set. In the upper panels, the Ar basis is kept fixed, while the Co basis is varied. In the lower panels, vice versa.

Co-/Ar-basis	ΔE_{CoN+Ar}	ΔE_{CoN+}	E_b	ω_{lowest}	$\omega_{main,1}$	$\omega_{main,2}$	$\omega_{largest}$
min+*spd*/tier2	0.182	0.133	0.345	29	231	237	330
tier1/tier2	0.259	0.211	0.346	29	232	237	331
tier2/tier2	0.562	0.536	0.303	30	224	229	316
tier3/tier2	0.569	0.543	0.295	31	224	229	316
tier2/min+*spd*	0.560	-	0.285	27	224	229	316
tier2/tier1	0.562	-	0.295	30	223	228	316
tier2/tier2	0.562	-	0.303	30	224	229	316
tier2/tier3	0.562	-	0.306	30	224	229	316

Table B.5.: Convergence of the energy difference ΔE_{CoN+Ar} [eV] between the D_{2d}- and D_{2h} isomers of Co_4^+Ar as well as between the corresponding bare clusters ΔE_{CoN+} [eV], the Ar binding energy of the ground-state isomer D_{2d} of Co_4^+Ar and the lowest, largest and two main vibrational frequencies ω [cm^{-1}] of the D_{2d} isomer of Co_4^+Ar with respect to the basis sets.

In order to get quantitative results, a tier2 basis set for Co is obviously required, while for Ar the smaller tier1 basis set would be sufficient. Energy differences are then converged within 10 meV. The vibrational modes are accurate within 1 cm^{-1} and all bond distances are converged to 0.01 Å. In most of the studied cases, there are only few Ar atoms, typically even only one, compared to several Co atoms in the cluster. Consequently, the Ar basis contributes only a minor fraction to the overall computational time and is thus not critical. Therefore, we consistently chose a tier2 basis for both species. Since the bond distances are decently converged already at the level of the minimal+*spd* basis, this reduced basis set has been used for the basin-hopping sampling prior to the electronic structure study. However, one cannot trust the energetics at this level. We therefore postrelaxed all structural motifs identified during the sampling using the tier2 basis set, regardless of their energy differences.

Co-/Ar-basis	$\Delta E_{\mathrm{CoN+Ar}}$	ΔE_{Co}	E_{b}	ω_{lowest}	$\omega_{\mathrm{main,1}}$	$\omega_{\mathrm{main,2}}$	$\omega_{\mathrm{largest}}$
min+*spd*/tier2	0.556	0.701	0.127	16	222	261	308
tier1/tier2	0.586	0.736	0.128	17	224	263	309
tier2/tier2	0.442	0.559	0.116	15	212	251	295
tier3/tier2	0.441	0.555	0.110	14	213	251	295
tier2/min+*spd*	0.447	-	0.106	13	213	251	295
tier2/tier1	0.443	-	0.110	14	212	251	295
tier2/tier2	0.442	-	0.116	15	212	251	295
tier2/tier3	0.441	-	0.118	15	213	251	295

Table B.6.: Convergence of the energy difference $\Delta E_{\mathrm{CoN+Ar}}$ [eV] between the D_{3d} and C_{2v} isomers of Co_6^+Ar as well as between the corresponding bare clusters $\Delta E_{\mathrm{CoN+}}$ [eV], the Ar binding energy of the ground-state isomer D_{3d} of Co_6^+Ar and the lowest, largest and two main vibrational frequencies ω [cm^{-1}] of the D_{3d} isomer of Co_6^+Ar with respect to the basis sets.

Co-/Ar-basis	r_1	r_2	r_3	r_4	r_5
min+*spd*/tier2	2.52	2.50	2.18	2.16	2.42
tier1/tier2	2.50	2.49	2.16	2.14	2.42
tier2/tier2	2.51	2.49	2.18	2.16	2.45
tier3/tier2	2.51	2.49	2.18	2.17	2.45
tier2/min+*spd*	2.51	2.49	2.18	2.16	2.47
tier2/tier1	2.51	2.49	2.18	2.16	2.45
tier2/tier2	2.51	2.49	2.18	2.17	2.45
tier2/tier3	2.51	2.49	2.18	2.17	2.45

Table B.7.: Convergence of the bond distances [Å] with respect to the basis sets for the ground-state isomer D_{2d} of Co_4^+Ar.

Co-/Ar-basis	r_1	r_2	r_3	r_4
min+*spd*/tier2	2.37	2.27	2.26	2.76
tier1/tier2	2.35	2.25	2.24	2.74
tier2/tier2	2.37	2.27	2.26	2.76
tier3/tier2	2.37	2.27	2.26	2.76
tier2/min+*spd*	2.37	2.27	2.26	2.76
tier2/tier1	2.37	2.27	2.26	2.76
tier2/tier2	2.37	2.27	2.26	2.76
tier2/tier3	2.37	2.27	2.26	2.74

Table B.8.: Convergence of the bond distances [Å] with respect to the basis sets for the ground-state isomer D_{3d} of Co_6^+Ar.

B.3. Cutoff Radius

The cutoff radius r_{cut} is varied over the range of 3 to 6 Å. The results are summarized in Tables B.9, B.10, B.11, B.12 and Fig. B.4.

Co-/Ar-r_{cut}	$\Delta E_{\mathrm{CoN+Ar}}$	$\Delta E_{\mathrm{CoN+}}$	E_{b}	ω_{lowest}	$\omega_{\mathrm{main,1}}$	$\omega_{\mathrm{main,2}}$	$\omega_{\mathrm{largest}}$
3 / 5	0.567	0.542	0.298	31	224	229	316
4 / 5	0.562	0.536	0.302	30	224	229	316
5 / 5	0.562	0.536	0.303	30	224	229	316
6 / 5	0.562	0.536	0.303	30	224	229	316
5 / 3	0.562	-	0.299	30	224	229	316
5 / 4	0.562	-	0.303	30	224	229	316
5 / 5	0.562	-	0.303	30	224	229	316
5 / 6	0.562	-	0.303	30	224	229	316

Table B.9.: Convergence of the energy difference $\Delta E_{\mathrm{CoN+Ar}}$ [eV] between the D_{2d} and D_{2h} isomers of Co_4^+Ar as well as between the corresponding bare clusters $\Delta E_{\mathrm{CoN+}}$ [eV], the Ar binding energy of the ground-state isomer D_{2d} of Co_4^+Ar and the lowest, largest and two main vibrational frequencies ω [cm^{-1}] of the D_{2d} isomer of Co_4^+Ar with respect to the cutoff radius r_{cut} [Å].

Co-/Ar-r_{cut}	$\Delta E_{\mathrm{CoN+Ar}}$	$\Delta E_{\mathrm{CoN+}}$	E_{b}	ω_{lowest}	$\omega_{\mathrm{main,1}}$	$\omega_{\mathrm{main,2}}$	$\omega_{\mathrm{largest}}$
3 / 5	0.439	0.558	0.112	14	213	252	296
4 / 5	0.442	0.559	0.115	15	212	251	295
5 / 5	0.442	0.559	0.116	15	212	251	295
6 / 5	0.442	0.559	0.116	15	212	251	295
5 / 3	0.442	-	0.112	15	212	251	295
5 / 4	0.442	-	0.115	15	212	251	295
5 / 5	0.442	-	0.116	15	212	251	295
5 / 6	0.442	-	0.116	15	212	251	295

Table B.10.: Convergence of the energy difference $\Delta E_{\mathrm{CoN+Ar}}$ [eV] between the D_{3d} and C_{2v} isomers of Co_6^+Ar as well as between the corresponding bare clusters ΔE_{Co} [eV], the Ar binding energy of the ground-state isomer D_{3d} of Co_6^+Ar and the lowest, largest and two main vibrational frequencies ω [cm^{-1}] of the D_{3d} isomer of Co_6^+Ar with respect to the cutoff radius r_{cut} [Å].

All results are tightly converged up to 2 meV, 1 cm^{-1} and 0.01 Å already at $r_{\mathrm{cut}} = 4$ Å and decently converged up to 10 meV, 2 cm^{-1} and 0.01 Å with $r_{\mathrm{cut}} = 3$ Å. Therefore, our conservatively chosen value of 5 Å provides tight convergence of all quantities at the tier2 basis set level.

Co-/Ar-r_{cut}	r_1	r_2	r_3	r_4	r_5
3 / 5	2.51	2.49	2.18	2.16	2.45
4 / 5	2.51	2.49	2.18	2.16	2.45
5 / 5	2.51	2.49	2.18	2.16	2.45
6 / 5	2.51	2.49	2.18	2.16	2.45
5 / 3	2.51	2.49	2.18	2.16	2.45
5 / 4	2.51	2.49	2.18	2.16	2.45
5 / 5	2.51	2.49	2.18	2.16	2.45
5 / 6	2.51	2.49	2.18	2.16	2.45

Table B.11.: Convergence of the bond distances [Å] with respect to the cutoff radius r_{cut} [Å] for the ground-state isomer D_{2d} of Co_4^+Ar.

Co-/Ar-r_{cut}	r_1	r_2	r_3	r_4
3 / 5	2.37	2.27	2.26	2.76
4 / 5	2.37	2.27	2.26	2.76
5 / 5	2.37	2.27	2.26	2.76
6 / 5	2.37	2.27	2.26	2.76
5 / 3	2.37	2.27	2.26	2.76
5 / 4	2.37	2.27	2.26	2.76
5 / 5	2.37	2.27	2.26	2.76
5 / 6	2.37	2.27	2.26	2.76

Table B.12.: Convergence of the bond distances [Å] with respect to the cutoff radius r_{cut} [Å] for the ground-state isomer D_{3d} of Co_6^+Ar.

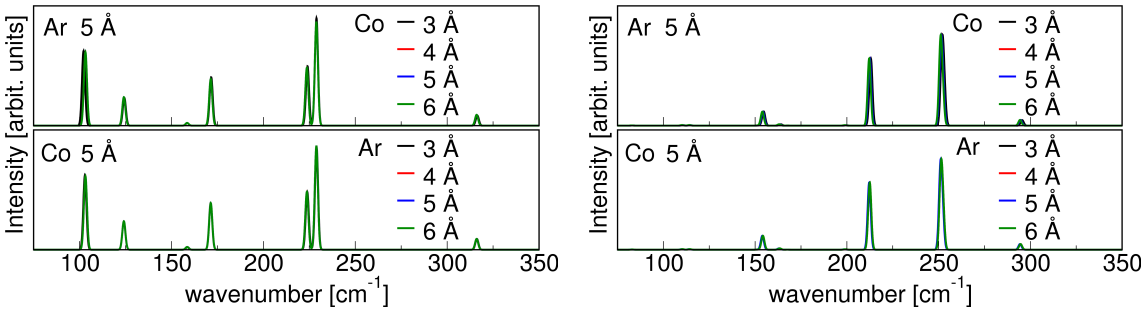

Figure B.4.: IR spectrum of the ground state of Co_4^+Ar (left panels) and Co_6^+Ar (right panels) vs. cutoff radius r_{cut}. In the upper panels, the Ar cutoff radius is kept fixed, while the Co cutoff radius is varied. In the lower panels, vice versa.

B.4. Hartree Potential

For the maximum angular momentum $l_{\max}$ in the multipole decomposition scheme, we tried a value of 3, 4, 6 and 8. The results are summarized in Tables B.13, B.14, B.15, B.16 and Fig. B.4.

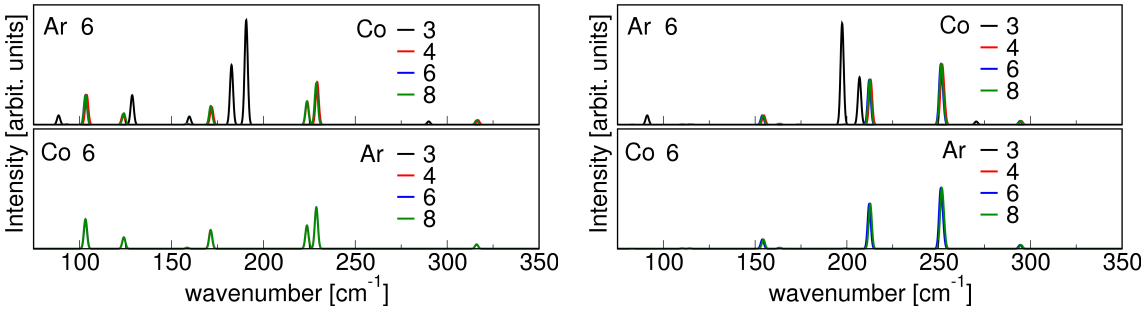

Figure B.5.: IR spectrum of the ground state of Co_4^+Ar (left panels) and Co_6^+Ar (right panels) vs. $l_{\max}$. In the upper panels, the Ar $l_{\max}$ is kept fixed, while the Co $l_{\max}$ is varied. In the lower panels, vice versa.

Co-/Ar-$l_{\max}$	$\Delta E_{\mathrm{CoN+Ar}}$	$\Delta E_{\mathrm{CoN+}}$	E_{b}	ω_{lowest}	$\omega_{\mathrm{main,1}}$	$\omega_{\mathrm{main,2}}$	$\omega_{\mathrm{largest}}$
3 / 6	0.219	0.191	0.298	27	183	191	290
4 / 6	0.561	0.536	0.303	26	224	229	317
6 / 6	0.562	0.536	0.303	30	224	229	316
8 / 6	0.562	0.536	0.303	30	224	229	316
6 / 3	0.562	-	0.303	30	224	229	316
6 / 4	0.562	-	0.303	30	224	229	316
6 / 6	0.562	-	0.303	30	224	229	316
6 / 8	0.562	-	0.303	30	224	229	316

Table B.13.: Convergence of the energy difference $\Delta E_{\mathrm{CoN+Ar}}$ [eV] between the D_{2d} and D_{2h} isomers of Co_4^+Ar as well as between the corresponding bare clusters $\Delta E_{\mathrm{CoN+}}$ [eV], the Ar binding energy of the ground-state isomer D_{2d} of Co_4^+Ar and the lowest, largest and two main vibrational frequencies ω [cm^{-1}] of the D_{2d} isomer of Co_4^+Ar with respect to $l_{\max}$.

A value of 3 for $l_{\max}$ is obviously too small, the energy differences are tenths of eV off. Bond distances are not converged within several hundredths of Å. Furthermore, the IR spectra do change a lot with increasing $l_{\max}$. The C_{2v} isomer of Co_6^+ could not even be converged with $l_{\max} = 3$. With a value of 4, however, tight convergence can be achieved. For Ar, $l_{\max}$ is not critical, since the density sitting on the single Ar atom contributes only little to the complete density. However, the contribution to the computational time is, like in the case of the basis set, not critical. We therefore chose for both species a conservative value of 6, for which tight convergence also for Co_4+Ar is achieved, where little noise was still observed for $l_{\max} = 4$.

Co-/Ar-l_{max}	ΔE_{CoN+Ar}	ΔE_{Co}	E_b	ω_{lowest}	$\omega_{main,1}$	$\omega_{main,2}$	$\omega_{largest}$
3 / 6	N./A.	N./A.	0.096	3	197	207	271
4 / 6	0.442	0.559	0.116	15	213	251	295
6 / 6	0.442	0.559	0.116	15	212	251	295
8 / 6	0.442	0.559	0.116	15	212	251	295
6 / 3	0.442	-	0.116	15	212	251	295
6 / 4	0.442	-	0.116	15	212	251	295
6 / 6	0.442	-	0.116	15	212	251	295
6 / 8	0.442	-	0.116	15	212	251	295

Table B.14.: Convergence of the energy difference ΔE_{CoN+Ar} [eV] between the D_{3d} and C_{2v} isomers of Co_6^+Ar as well as between the corresponding bare clusters ΔE_{CoN+} [eV], the Ar binding energy of the ground-state isomer D_{3d} of Co_6^+Ar and the lowest, largest and two main vibrational frequencies ω [cm^{-1}] of the D_{3d} isomer of Co_6^+Ar with respect to l_{max}.

Co-/Ar-l_{max}	r_1	r_2	r_3	r_4	r_5
3 / 6	2.51	2.49	2.21	2.20	2.44
4 / 6	2.51	2.49	2.18	2.16	2.45
6 / 6	2.51	2.49	2.18	2.16	2.45
8 / 6	2.51	2.49	2.18	2.17	2.45
6 / 3	2.51	2.49	2.18	2.16	2.45
6 / 4	2.51	2.49	2.18	2.16	2.45
6 / 6	2.51	2.49	2.18	2.16	2.45
6 / 8	2.51	2.49	2.18	2.16	2.45

Table B.15.: Convergence of the bond distances [Å] with respect to l_{max} for the ground-state isomer D_{2d} of Co_4^+Ar.

Co-/Ar-l_{max}	r_1	r_2	r_3	r_4
3 / 6	2.42	2.41	2.30	2.84
4 / 6	2.37	2.27	2.26	2.76
6 / 6	2.37	2.27	2.26	2.76
8 / 6	2.37	2.27	2.26	2.76
6 / 3	2.37	2.27	2.26	2.76
6 / 4	2.37	2.27	2.26	2.76
6 / 6	2.37	2.27	2.26	2.76
6 / 8	2.37	2.27	2.26	2.76

Table B.16.: Convergence of the bond distances [Å] with respect to l_{max} for the ground-state isomer D_{3d} of Co_6^+Ar.

B.5. Force Convergence Criterium and Finite Displacement for the Numerical Hessian and Dipole Gradient

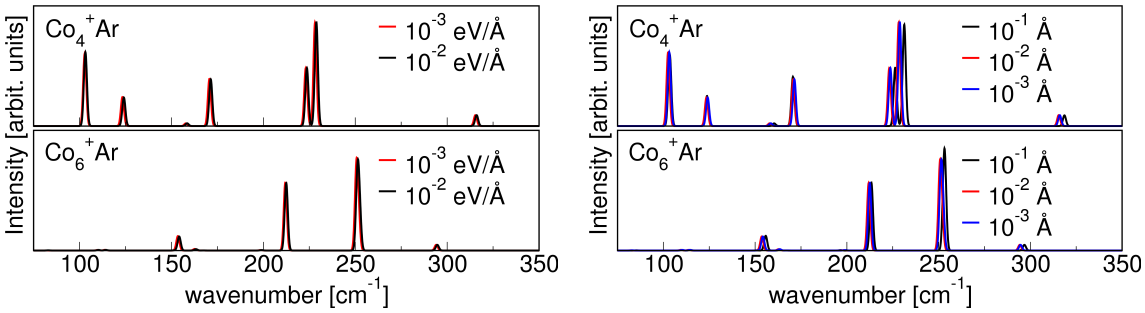

Figure B.6.: IR spectrum of the ground state of Co_4^+Ar and Co_6^+Ar vs. force convergence criterium $F_{\max}$ (left panels) and finite displacement Δ (right panels).

Though the bond distances, as was illustrated in section 6.2, are typically converged within 10^{-3} Å using a force convergence criterium for the local relaxation scheme of 10^{-2} eV/Å, it is *a priori* not clear, whether such a value is enough to converge the vibrational frequencies and IR spectra, for which it is essential to be in a local minimum. We therefore further relaxed the ground-state isomers of Co_4^+Ar and Co_6^+Ar further to a tighter force convergence criterium of 10^{-3} eV/Å and recomputed the IR spectra, which are presented in the left panel of Fig. B.6. As one can see, the IR spectra do not change at all. The step width Δ for the finite difference scheme to calculate the Hessian and dipole gradient numerically turns out to be uncritical (see the right panel of Fig. B.6). Our chosen value of 10^{-3} Å is small enough, ensuring a converged IR spectrum without showing grid noise due to the discrete integration grid.

C. Convergence Tests for Si and Cu clusters

The technical parameters to converge together with their default values in brackets are:

1. The integration grid which is determined by $N_{\mathrm{r,div}}$ (2) and $N_{\mathrm{ang,max}}$ (302). Cf. section 5.3.
2. The basis set (minimal+*spd*). Cf. section 5.2.
3. The cutoff radius r_{cut} (4 Å). Cf. section 5.2.
4. The maximum angular momentum in the multipole decomposition of the Hartree potential l_{max} (6). Cf. section 5.4.
5. The force convergence criterium F_{max} (10^{-2} eV/Å). Cf. section 6.2.
6. The step width Δ (10^{-3} Å) for the finite displacement to calculate the Hessian. Cf. section 6.3.

For the ensuing convergence tests, each parameter is in turn individually varied whereas for the other parameters the default value is used and kept fixed. As will be shown below, these default settings are sufficiently converged for the purpose of the intended study and have therefore been used in the production runs. All tests are done using the PBE functional with a Gaussian smearing of 0.1 eV width consistent to the production runs (see section 9.2). For the convergence tests, it is crucial to choose proper target quantities with respect to which the settings have to be converged, which in turn depends upon the actual problem to tackle. The focus of the study here lies in the sampling performance. Tightly converged physical quantities are therefore not crucial. Important are instead the right energetic order of the isomers and the correct structural motifs. We therefore check the energy differences with respect to the atomization energy

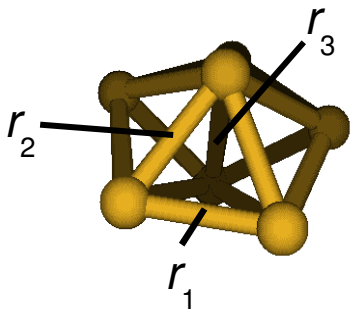

Figure C.1.: Pentagonal bipyramid motif of Si_7 and Cu_7 together with labelled bonds used for the convergence tests.

$$E_{\mathrm{at}} = E_{\mathrm{tot}}(X_N) - NE_{\mathrm{tot}}(X) \ . \tag{C.1}$$

of the ground state (X=Si, Cu) as well as the bond distances. The vibrational frequencies are important for the vibrational stability analysis. The convergence tests focus on the dominant isomers of Si_7 and Cu_7 (cf. section 9.3.1) concerning the energy difference. Bond distances, as well as the smallest and largest vibrational frequency are only given for the D_{5h} ground-state isomer.

C.1. Integration Grid

The angular part of the integration grid $N_{\mathrm{ang,max}}$ is varied over several different Lebedev-grids, that are 194, 302, 434, 590 and 770. Using 302 the radial part which is determined by $N_{\mathrm{r,div}}$ is augmented from 2 to 4. The convergence tests are summarized in Tables C.1 and C.2.

grid	E_{at}	$\Delta E(\#2)$	$\Delta E(\#3)$	$\Delta E(\#4)$	r_1	r_2	r_3	$\omega_{\mathrm{smallest}}$	$\omega_{\mathrm{largest}}$
(194/2)	-31.362	0.780	0.957	0.968	2.51	2.49	2.55	170	435
(302/2)	-31.361	0.782	0.956	0.965	2.51	2.49	2.55	171	435
(434/2)	-31.362	0.782	0.959	0.966	2.51	2.49	2.55	171	435
(590/2)	-31.363	0.782	0.958	0.967	2.51	2.49	2.55	170	435
(770/2)	-31.363	0.782	0.958	0.967	2.51	2.49	2.55	170	435
(302/4)	-31.361	0.782	0.956	0.965	2.51	2.49	2.55	171	435

Table C.1.: Convergence of the atomization energy E_{at} [eV] and energy differences w.r.t. the ground state ΔE [eV] for the four dominant isomers of Si_7 as well as the bond distances, smallest and largest vibrational frequency [cm^{-1}] of the ground state w.r.t. the integration grid ($N_{\mathrm{ang,max}}/N_{\mathrm{r,div}}$).

grid	E_{at}	$\Delta E(\#2)$	$\Delta E(\#10)$	r_1	r_2	r_3	$\omega_{\mathrm{smallest}}$	$\omega_{\mathrm{largest}}$
(194/2)	-14.701	0.225	1.105	2.46	2.46	2.60	70	240
(302/2)	-14.700	0.223	1.103	2.46	2.46	2.60	70	240
(434/2)	-14.699	0.222	1.103	2.46	2.46	2.60	70	240
(590/2)	-14.699	0.222	1.103	2.46	2.46	2.60	70	240
(770/2)	-14.699	0.222	1.103	2.46	2.46	2.60	70	240
(302/4)	-14.700	0.223	1.103	2.46	2.46	2.60	70	240

Table C.2.: Convergence of the atomization energy E_{at} [eV] and energy differences w.r.t. the ground state ΔE [eV] for the three dominant isomers of Cu_7 as well as the bond distances, smallest and largest vibrational frequency [cm^{-1}] of the ground state w.r.t. the integration grid ($N_{\mathrm{ang,max}}/N_{\mathrm{r,div}}$).

The integration grids are not critical at all and all quantities are tightly converged using the default value of (302/2).

C.2. Basis Set Convergence

The basis set composition is given in Appendix A. The convergence tests are summarized in Tables C.3 and C.4.

basis	E_{at}	$\Delta E(\#2)$	$\Delta E(\#3)$	$\Delta E(\#4)$	r_1	r_2	r_3	$\omega_{\mathrm{smallest}}$	$\omega_{\mathrm{largest}}$
min	-23.715	0.446	N./A.	0.618	2.78	2.79	2.95	114	346
min+*spd*	-31.361	0.782	0.956	0.965	2.51	2.49	2.55	171	435
tier1	-31.669	0.798	0.985	0.990	2.50	2.48	2.54	172	438
tier2	-31.788	0.784	0.977	0.986	2.50	2.47	2.52	172	437
tier3	-31.817	0.782	0.973	0.984	2.50	2.47	2.52	172	437

Table C.3.: Convergence of the atomization energy E_{at} [eV] and energy differences w.r.t. the ground state ΔE [eV] for the four dominant isomers of Si_7 as well as the bond distances, smallest and largest vibrational frequency [cm^{-1}] of the ground state w.r.t. the basis set.

basis	E_{at}	$\Delta E(\#2)$	$\Delta E(\#10)$	r_1	r_2	r_3	$\omega_{\mathrm{smallest}}$	$\omega_{\mathrm{largest}}$
min	-9.507	0.007	0.325	2.61	2.76	3.28	60	171
min+*spd*	-14.700	0.223	1.103	2.46	2.46	2.60	70	240
tier1	-14.906	0.226	1.097	2.45	2.45	2.57	71	240
tier2	-14.991	0.228	1.110	2.45	2.45	2.57	71	241
tier3	-15.030	0.231	1.118	2.45	2.45	2.57	71	241

Table C.4.: Convergence of the atomization energy E_{at} [eV] and energy differences w.r.t. the ground state ΔE [eV] for the three dominant isomers of Cu_7 as well as the bond distances, smallest and largest vibrational frequency [cm^{-1}] of the ground state w.r.t. the basis set.

Though tight convergence up to a few meV in the energy differences and 0.01 Å in the bond distances can only be achieved using a tier2 basis, the energetic order is already correct using a minimal+*spd* basis. Bond distances are converged within a few hundreds Å, so that the structural motifs are established. We therefore chose the reduced minimal+*spd* basis for the sampling performance analysis.

C.3. Cutoff Radius

The cutoff radius r_{cut} is varied over the range of 3 to 6 Å. The results are summarized in Tables C.5 and C.6.

r_{cut}	E_{at}	$\Delta E(\#2)$	$\Delta E(\#3)$	$\Delta E(\#4)$	r_1	r_2	r_3	ω_{smallest}	ω_{largest}
3	-31.198	0.786	0.953	0.966	2.51	2.49	2.55	170	434
4	-31.361	0.782	0.956	0.965	2.51	2.49	2.55	171	435
5	-31.368	0.782	0.956	0.964	2.51	2.49	2.55	170	435
6	-31.368	0.782	0.956	0.964	2.51	2.49	2.55	170	435

Table C.5.: Convergence of the atomization energy E_{at} [eV] and energy differences w.r.t. the ground state ΔE [eV] for the four dominant isomers of Si_7 as well as the bond distances, smallest and largest vibrational frequency [cm^{-1}] of the ground state w.r.t. r_{cut} [Å].

r_{cut}	E_{at}	$\Delta E(\#2)$	$\Delta E(\#10)$	r_1	r_2	r_3	ω_{smallest}	ω_{largest}
3	-14.510	0.222	1.081	2.46	2.46	2.60	70	240
4	-14.700	0.223	1.103	2.46	2.46	2.60	70	240
5	-14.723	0.224	1.107	2.46	2.46	2.60	70	239
6	-14.725	0.224	1.108	2.46	2.46	2.60	70	239

Table C.6.: Convergence of the atomization energy E_{at} [eV] and energy differences w.r.t. the ground state ΔE [eV] for the three dominant isomers of Cu_7 as well as the bond distances, smallest and largest vibrational frequency [cm^{-1}] of the ground state w.r.t. r_{cut} [Å].

The bond distances do not vary at all over the range of the considered cutoff radii. Furthermore, the energy differences are converged within 10 meV and the vibrational frequencies within 2 cm^{-1} at $r_{\text{cut}} = 4$ Å so that we chose this value for the production runs.

C.4. Hartree Potential

For the maximum angular momentum $l_{\max}$ in the multipole decomposition scheme, we tried a value of 3, 4, 6 and 8. The results are summarized in Tables C.7 and C.8.

$l_{\max}$	E_{at}	$\Delta E(\#2)$	$\Delta E(\#3)$	$\Delta E(\#4)$	r_1	r_2	r_3	$\omega_{\mathrm{smallest}}$	$\omega_{\mathrm{largest}}$
3	-31.369	0.779	0.954	0.961	2.51	2.49	2.55	170	435
4	-31.365	0.781	0.956	0.964	2.51	2.49	2.55	170	435
6	-31.361	0.782	0.956	0.965	2.51	2.49	2.55	171	435
8	-31.361	0.782	0.956	0.965	2.51	2.49	2.55	170	435

Table C.7.: Convergence of the atomization energy E_{at} [eV] and energy differences w.r.t. the ground state ΔE [eV] for the four dominant isomers of Si_7 as well as the bond distances, smallest and largest vibrational frequency [cm^{-1}] of the ground state w.r.t. $l_{\max}$.

$l_{\max}$	E_{at}	$\Delta E(\#2)$	$\Delta E(\#10)$	r_1	r_2	r_3	$\omega_{\mathrm{smallest}}$	$\omega_{\mathrm{largest}}$
3	-14.713	0.223	1.104	2.46	2.46	2.60	70	240
4	-14.704	0.223	1.104	2.46	2.46	2.60	70	240
6	-14.700	0.223	1.103	2.46	2.46	2.60	70	240
8	-14.700	0.223	1.103	2.46	2.46	2.60	70	240

Table C.8.: Convergence of the atomization energy E_{at} [eV] and energy differences w.r.t. the ground state ΔE [eV] for the three dominant isomers of Cu_7 as well as the bond distances, smallest and largest vibrational frequency [cm^{-1}] of the ground state w.r.t. $l_{\max}$.

Again, the results do not critically depend upon $l_{\max}$ and with the default value of 6, all results are converged within 1 meV, 0.01 Å and 1 cm^{-1} at the minimal+*spd* basis set level.

C.5. Force Convergence Criterium and Finite Displacement for the Numerical Hessian

		Si_7		Cu_7	
		ω_{smallest}	ω_{largest}	ω_{smallest}	ω_{largest}
F_{max} [eV/Å]	10^{-2}	170	435	70	240
	10^{-3}	170	435	70	240
Δ [Å]	10^{-1}	170	437	70	241
	10^{-2}	170	435	70	240
	10^{-3}	170	435	70	240

Table C.9.: Vibrational frequencies for the ground-state isomers of Si_7 and Cu_7 w.r.t. the force convergence criterium F_{max} and the finite displacement Δ.

Though the bond distances, as was illustrated in section 6.2, are typically converged within 10^{-3} Å using a force convergence criterium for the local relaxation scheme of 10^{-2} eV/Å, it is *a priori* not clear, whether such a value is enough to converge the vibrational frequencies, for which it is essential to be in a local minimum. We therefore further relaxed the ground-state isomers of Si_7 and Cu_7 further to a tighter force convergence criterium of 10^{-3} eV/Å and recomputed the vibrational spectra, of which the smallest and largest frequencies are presented in Table C.9. As one can see, the frequencies do not change at all. The step width Δ for the finite difference scheme to calculate the Hessian turns out to be uncritical. Our chosen value of 10^{-3} Å is small enough, ensuring a converged vibrational spectrum without showing grid noise due to the discrete integration grid.

D. High Order Finite Difference Schemes

Numerical derivatives are required for the calculation of the Hessian, which is composed of the first derivatives of the atomic forces. Furthermore, numerical forces are used as reference values for the accuracy tests of analytical forces. Accurate high-order schemes up to any desired order can herein be obtained by a Taylor-expansion.

$$\frac{\partial}{\partial x} f = \frac{1}{\tilde{C}h} \sum_{n=-N}^{N} C_n f(x_i + nh, y_j, z_k) + O(h^{2N}) \; . \tag{D.1}$$

The coefficients are anti-symmetric with respect to the central node $f(x_i, y_j, z_k)$, i.e. $C_{-n} = -C_n$ and are given in Table D.1.

N	$\tilde{C}$	C_3	C_2	C_1	C_0
1	2			1	0
2	12		-1	8	0
3	60	1	-9	45	0

Table D.1.: Coefficients for the first numerical derivative

N	$\tilde{C}$	C_6	C_5	C_4	C_3	C_2	C_1	C_0
1	1						1	-2
2	12					-1	16	-30
3	180				2	-27	270	-490
4	5040			-9	128	-1008	8064	-14350
5	25200		8	-125	1000	-6000	42000	-73766
6	831600	-50	864	-7425	44000	-222750	1425600	-2480478

Table D.2.: Coefficients for the second numerical derivative

Correspondingly, the second derivative can be discretized

$$\frac{\partial^2}{\partial x^2}\phi = \frac{1}{\tilde{C}h^2}\sum_{n=-N}^{N} C_n \phi(x_i + nh, y_j, z_k) + O(h^{2N+2}) \; . \tag{D.2}$$

Here, the coefficients (Table D.2) are symmetric, i.e. $C_{-n} = C_n$.